Arch. Mech., **51**, 6, pp. 665–692, Warszawa 1999

Multiaxial constitutive modelling for R-phase and M-phase transformations of TiNi shape memory alloys

M. KAWAI, H. OGAWA, V. BABURAJ, and T. KOGA

Institute of Engineering Mechanics and Systems,
University of Tsukuba, Tsukuba 305-8573, JAPAN
e-mail: mkawai@kz.tsukuba.ac.jp

A MULTIAXIAL CONSTITUTIVE MODEL for describing the pseudoelastic and shape memory behaviour of a titanium-nickel (TiNi) shape memory alloy due to the stress-induced rhombohedral and martensitic transformations has been developed from a phenomenological point of view. First, the existing constitutive models proposed for shape memory alloys are reviewed in brief. On the basis of a comparison between these models, an expression prescribing the transformation strain range is proposed which depends on the applied stress and the current phase volume fraction. Then, the uniaxial Tanaka model for the rhombohedral and martensitic transformations of TiNi shape memory alloys is extended to a multiaxial form using the framework of the Boyd-Lagoudas model and the proposed expression of the transformation strain range. Finally, the capability of the present model to predict the pseudoelastic behaviour of TiNi shape memory alloys is examined through numerical simulations of stress-strain responses under uniaxial and multiaxial proportional/nonproportional loading-unloading conditions.

1. Introduction

SHAPE MEMORY ALLOY (SMA) BASED SMART STRUCTURES are typically fabricated of composite materials embedding fibres, films or particles of SMAs [1 – 8]. For optimum designs of SMA composite laminae, laminates and structures, it is required to evaluate the fabrication conditions under which the pseudoelasticity (PE) and the shape memory effect (SME) of SMA are reflected and the thermomechanical conditions under which SMA composites appropriately work as intended. To design the performance characteristics, a suitable numerical simulation technique should be developed. To this end, it is prerequisite to establish constitutive models for describing the transformation behaviour of SMA embedded in matrix materials. The local states of stress and strain of the embedded SMA always become multiaxial and the phase transformations are believed to be very sensitive to complex combined states of stress and strain. For advanced designs of SMA smart composites, therefore, it is one of the most significant tasks

http://rcin.org.pl

to formulate a constitutive model which accurately describes the SME and the nonlinear PE, including the changes in stiffness and energy dissipation property, of SMAs under arbitrary multiaxial thermomechanical loading conditions.

To describe the pseudoelastic and shape memory behaviour of SMA under uniaxial loading conditions, TANAKA *et al.* [9 – 12] developed rate-form constitutive relations from phenomenological points of view. A fundamental version of the Tanaka model is very useful in practice for a description of the martensitic transformation of SMA. It has a relatively simple structure and the material constants involved can be easily identified. For this reason, this model is frequently used in reporting experimental results on the stress-strain behaviour of SMAs [13 – 16]. Tanaka's pioneering works stimulated the subsequent development in the constitutive modelling of the transformation behaviour of SMAs. LIANG and ROGERS applied a finite form of the Tanaka model which was combined with a slightly different expression of the transformation kinetics [17]. An extension of the Tanaka model was also discussed by BRINSON [18]. Other different formulations were presented by MULLER and XU [19], GRAESSER and COZZARELLI [20], IVSHIN and PENCE [21, 22], ABEYARATNE *et al.* [23] and BARRETT [24].

A multiaxial phenomenological modelling of the martensitic transformation behaviour of SMAs was first discussed by LIANG and ROGERS [25]. This model was based on the classical plasticity and the uniaxial Tanaka model, and an isotropic transformation criterion of von Mises type was assumed. A change in the elastic property due to phase transformation was not considered. An improved multiaxial version which accounted for the change in stiffness due to the martensitic transformation was developed by BOYD and LAGOUDAS [26, 27], also using the von Mises equivalent stress and the framework of the Tanaka model. RANIECKI *et al.* [28] and RANIECKI and LEXCELLENT [29] developed three-dimensional pseudoelasticity models which furnished rigorous loading-unloading criteria for the forward and reverse martensitic transformations and a capability to describe the change in elastic modulus due to phase evolution. Validity of these pseudoelasticity models were evaluated by ROGUEDA *et al.* [30] through combined tension-torsion tests. GRAESSER and COZZARELLI [31] also attempted to develop a multiaxial SMA model using a different framework. BRINSON and HUANG [32] made a comparison between Tanaka, Liang-Rogers, Brinson, Ivshin-Pense and Boyd-Lagoudas models. From this comparison, it was elucidated that these SMA models exhibited many similarities, and essential differences appeared in the formulation of the transformation kinetics. Physically-based micromechanical formulations which took into account the crystallographic growth of twin variants and their movements were developed by PATOOR *et al.* [33, 34] and SUN and HWANG [35, 36]. More detailed reviews on the constitutive modelling of the pseudoelastic and shape memory behaviour can be found in the articles given by FISCHER *et al.* [37] and BIRMAN [38].

http://rcin.org.pl

Experimental results on the multiaxial stress-strain behaviour of SMAs have not been sufficiently reported so far [30, 39, 40]. For this reason, a stress criterion of the multiaxial phase transformation of SMAs is not completely understood, and the transformation kinetics assumed in developing the SMA models is not fully justified. To remove this insufficiency, systematic experiments to elucidate the multiaxial transformation kinetics of SMAs should be programmed. In parallel with experimental efforts, additional investigations will also be required on the theoretical sophistication of existing multiaxial SMA constitutive models as well as new developments from different points of view. Recently, experimental data on the uniaxial stress-strain behaviour of SMAs under tensile and compressive loading conditions are increasingly reported in literature. This has partly eliminated some difficulties in determining the material constants involved by the phenomenological constitutive models. Therefore, we are now able to promote further basic studies for examining the applicability of existing SMA models and for developing multiaxial SMA constitutive models, irrespective of a limited amount of information on the transformation behaviour of SMAs under general thermomechanical loading conditions.

A titanium-nickel (TiNi) shape memory alloy is a promising candidate for practical applications, since its characteristic performance is presently superior to other existing SMAs [41]. It is a characteristic of TiNi SMA that the rhombohedral (R-phase) transformation occurs in a particular temperature range before the martensitic (M-phase) transformation starts, which depends on the heat treatment [42]. Since the R-phase transformation takes place at a lower stress, the pseudoelastic and shape memory behaviour due to the R-phase transformation are more stable under repeated application. The consecutive R-phase and M-phase transformations are believed to have a significant influence on the stress-strain curves for TiNi SMA. To design TiNi-SMA fibre (or particle) embedded composites and to evaluate their performance characteristics under arbitrary thermomechanical loading conditions, a multiaxial SMA constitutive model for describing the R-phase and M-phase transformations of TiNi SMAs is required. However, a three-dimensional modelling of the R-phase and M-phase transformations occurring in TiNi SMAs has not been discussed so far, and effects of the R-phase transformation on the multiaxial behaviour of SMA have not been studied through numerical simulations.

The objective of the present study is to develop a multiaxial constitutive model for describing the stress-induced R-phase and M-phase transformations in TiNi SMA from a phenomenological point of view. First, the uniaxial TANAKA model [11] and the multiaxial BOYD and LAGOUDAS model [26] are briefly discussed. On the basis of a comparison between these models, an expression of the transformation strain range is proposed. Then, the uniaxial Tanaka model for the R-phase and M-phase transformations of TiNi SMAs is extended into a

http://rcin.org.pl

multiaxial form by applying the framework of the Boyd-Lagoudas model together with the proposed expression of the transformation strain range. To examine the capability of the present model for TiNi SMAs, the stress-induced phase transformation behaviour is numerically simulated for various uniaxial and multiaxial proportional/nonproportional loading-unloading conditions.

2. Phenomenological SMA constitutive models

2.1. Uniaxial Tanaka model for M-phase transformation

The basic rate equation of the uniaxial Tanaka model for the M-phase transformation [9 – 12] is expressed as

$$\dot{\sigma} = D\dot{\varepsilon} + \Theta\dot{T} + \Omega\dot{\xi}, \tag{2.1}$$

where σ, ε and T denote the uniaxial stress, the infinitesimal total strain and the absolute temperature, and ξ is the volume fraction of M-phase. The coefficients D, Θ and Ω are material constants that represent the average Young's modulus, the thermal expansion coefficient and the modulus for the M-phase transformation. The dot $(\cdot)$ above the symbols represents the time rate.

The rate of the transformation strain $\varepsilon^{\mathrm{tr}}$ is described as

$$\dot{\varepsilon}^{\mathrm{tr}} = -\frac{\Omega}{D}\dot{\xi}, \tag{2.2}$$

where the coefficient $-\Omega/D$ is equivalent to the maximum transformation strain (when $\xi = 1$) caused by the stress-induced M-phase transformation.

The volume fraction ξ is a single internal variable which characterizes the M-phase transformation. The evolution equation of ξ is specified separately for the forward and reverse transformations, and it is described using the exponential form of MAGEE type [43]. LIANG and ROGERS [17] have integrated Eq. (2.1) and applied it to the analyses of smart structures.

2.2. Uniaxial Tanaka model for R-phase and M-phase transformations

In TiNi SMAs, the R-phase transformation occurs before the M-phase transformation starts in a particular range of temperature [41]. To describe the thermomechanical behaviour of TiNi SMAs due to these two kinds of consecutive phase transformations, LIN *et al.* [13] extended the Tanaka model, Eq. (2.1), to the following form:

$$\dot{\sigma} = D\dot{\varepsilon} + \Theta\dot{T} + K\dot{z}, \tag{2.3}$$

http://rcin.org.pl

where z represents the volume fractions η and ξ of R-phase and M-phase, respectively. Hence, the last term on the right-hand side of Eq. (2.3) is interpreted as

$$K\dot{z} = \begin{cases} \Psi\dot{\eta} & (\mathrm{R}-\mathrm{phase}) \\ \Omega\dot{\xi} & (\mathrm{M}-\mathrm{phase}) \end{cases}. \tag{2.4}$$

2.3. Multiaxial Boyd-Lagoudas model for M-phase transformation

The multiaxial SMA model proposed by BOYD and LAGOUDAS [26, 27] takes into account the changes in stiffness and thermal expansion coefficient during the martensitic phase transformation, and it considers the volumetric elastic strain. In this model, the rate of the deviatoric transformation strain $\dot{\varepsilon}_{ij}^{\mathrm{tr}}$ is expressed as

$$\dot{\varepsilon}_{ij}^{\mathrm{tr}} = \Lambda_{ij}\dot{\xi}, \tag{2.5}$$

where ξ is the volume fraction of M-phase, and Λ_{ij} represents the transformation tensor given by

$$\Lambda_{ij} = \begin{cases} \mathrm{HN}_{ij}^{\sigma}, & \dot{\xi} > 0, \\ \mathrm{HN}_{ij}^{\varepsilon}, & \dot{\xi} < 0 \end{cases}. \tag{2.6}$$

The flow directions N_{ij}^{σ} and N_{ij}^{ε} are specified as

$$N_{ij}^{\sigma} = \frac{3}{2}\frac{s_{ij}}{\sigma_e}, \tag{2.7}$$

$$N_{ij}^{\varepsilon} = \frac{\varepsilon_{ij}^{\mathrm{tr}}}{\varepsilon_e^{\mathrm{tr}}}, \tag{2.8}$$

for the forward and reverse transformations, respectively.

It is seen that the transformation flow takes place in the direction of the stress deviator during the forward transformation, and in the direction of the origin of the transformation strain during the reverse transformation. The coefficient H in Eq. (2.6) represents the maximum transformation strain attained when $\xi = 1$; $H = \varepsilon_{\max}^{\mathrm{tr}}$ under uniaxial tension.

The infinitesimal total strain ε_{ij} is given by the sum of the elastic, thermoelastic and phase transformation strains:

$$\varepsilon_{ij} = \varepsilon_{ij}^{e} + \varepsilon_{ij}^{T} + \varepsilon_{ij}^{\mathrm{tr}}, \tag{2.9}$$

where ε_{ij}^{e} and ε_{ij}^{T} denote the elastic and thermal expansion strain tensors. Using the Hooke's law, the constitutive relationship can be written as

$$\dot{\sigma}_{ij} = \overline{C_{ijkl}\varepsilon_{kl}^{e}} = C_{ijkl}\dot{\varepsilon}_{kl}^{e} + \dot{C}_{ijkl}\varepsilon_{kl}^{e}. \tag{2.10}$$

http://rcin.org.pl

To take into account the changes in the elastic tensor C_{ijkl} and the thermal expansion tensor α_{ij} of SMAs due to phase transformation, the rule of mixture is assumed:

$$C_{ijkl} = C^{\mathrm{A}}_{ijkl} + \xi \left(C^{\mathrm{M}}_{ijkl} - C^{\mathrm{A}}_{ijkl} \right), \tag{2.11}$$

$$\alpha_{ij} = \alpha^{\mathrm{A}}_{ij} + \xi \left(\alpha^{\mathrm{M}}_{ij} - \alpha^{\mathrm{A}}_{ij} \right), \tag{2.12}$$

where the superscripts A and M indicate the austenite and martensite, respectively.

Then, the constitutive relationship for the M-phase transformation is expressed as

$$\dot{\sigma}_{ij} = C_{ijkl} \left(\dot{\varepsilon}_{kl} - \alpha_{kl} \dot{T} \right) + Q_{ij} \dot{\xi}, \tag{2.13}$$

where

$$Q_{ij} = \left(C^{\mathrm{M}}_{ijkl} - C^{\mathrm{A}}_{ijkl} \right) \varepsilon^{e}_{kl} - C_{ijkl} \left(\alpha^{\mathrm{M}}_{kl} - \alpha^{\mathrm{A}}_{kl} \right) \Delta T - C_{ijkl} \Lambda_{kl}. \tag{2.14}$$

In Eq. (2.14), $\Delta T = T - T_0$ and T_0 is a reference temperature.

3. Transformation strain range

A description of the transformation strain range is an important part of modelling of the thermomechanical behaviour of SMAs. By comparing the Tanaka model and the Boyd-Lagoudas one for the M-phase transformation, we find the following correspondence:

$$C^{-1}_{11kl} Q_{kl} \leftrightarrow \frac{\Omega}{D}. \tag{3.1}$$

To examine this correspondence in more detail, we can use the following relationship:

$$C^{-1}_{ijkl} Q_{kl} = \frac{\kappa^{\mathrm{M}} - \kappa^{\mathrm{A}}}{9 \left[\kappa(\xi) \right]^2} \sigma_m \delta_{ij} + \frac{\mu^{\mathrm{M}} - \mu^{\mathrm{A}}}{2 \left[\mu(\xi) \right]^2} s_{ij} - \left(\alpha^{\mathrm{M}}_{ij} - \alpha^{\mathrm{A}}_{ij} \right) \Delta T - \Lambda_{ij}, \tag{3.2}$$

where σ_m and δ_{ij} are the mean stress $\sigma_{aa}/3$ and the Kronecker delta, respectively, and $\kappa(\xi)$ and $\mu(\xi)$ represent the bulk and shear moduli described as

$$\kappa(\xi) = (1 - \xi) \kappa^{\mathrm{A}} + \xi \kappa^{\mathrm{M}}, \tag{3.3}$$

$$\mu(\xi) = (1 - \xi) \mu^{\mathrm{A}} + \xi \mu^{\mathrm{M}}, \tag{3.4}$$

for the mixture of A-phase and M-phase.

Using this general relationship for isotropic SMAs, we can describe the coefficient $H (= \Lambda_{11})$ involved by the Boyd-Lagoudas model as follows:

$$H = -\frac{\Omega}{D} + \left[\frac{\kappa^{\mathrm{M}} - \kappa^{\mathrm{A}}}{9 \left[\kappa(\xi) \right]^2} + \frac{\mu^{\mathrm{M}} - \mu^{\mathrm{A}}}{3 \left[\mu(\xi) \right]^2} \right] \sigma - \left(\alpha^{\mathrm{M}} - \alpha^{\mathrm{A}} \right) \Delta T. \tag{3.5}$$

http://rcin.org.pl

The second and third terms on the right-hand side of Eq. (3.5) compensate for the constant stiffness and thermal expansion assumed in the uniaxial Tanaka model [9]. Experimental results for the uniaxial stress-strain behaviour of SMAs are often reported in terms of the coefficients Ω and D included by the uniaxial Tanaka model, e.g., [13]. To utilize the supplied information on the transformation strain range characterized by these coefficients in the calculations using the Boyd-Lagoudas model, the relationship given by Eq. (3.5) should be considered. In view of this requirement, the transformation strain range is newly defined as follows:

$$H^* = -\frac{\Omega^*}{E(\xi)} + \frac{E^{\mathrm{M}} - E^{\mathrm{A}}}{[E(\xi)]^2}\sigma_e - \left(\alpha^{\mathrm{M}} - \alpha^{\mathrm{A}}\right)\Delta T, \tag{3.6}$$

where a scalar quantity Ω^* is a history-dependent material parameter in general, and

$$E(\xi) = E^{\mathrm{A}} + \xi(E^{\mathrm{M}} - E^{\mathrm{A}}). \tag{3.7}$$

Note that $H^* = -\Omega/D$ when $E^{\mathrm{M}} = E^{\mathrm{A}} = D$, $\nu^{\mathrm{M}} = \nu^{\mathrm{A}}$, $\alpha^{\mathrm{M}} = \alpha^{\mathrm{A}}$ and $\Omega^* = \Omega$.

4. A description of multiaxial R-phase and M-phase transformation behaviour

A simple multiaxial SMA model for describing the R-phase and M-phase transformation behaviour of TiNi SMAs is developed on the basis of the uniaxial Tanaka model [9] and the multiaxial Boyd-Lagoudas model [26, 27]. In the following description, the superscripts (x, y) represent the pairs of (A, R), (R, M) or (A, M): A, austenitic phase; R, rhombohedral phase; M, martensitic phase. The changes in the elastic and thermoelastic properties due to the R-phase and M-phase transformations are considered through the rule of mixture, i.e.,

$$C_{ijkl}^{x\to y} = C_{ijkl}^{x} + z(C_{ijkl}^{y} - C_{ijkl}^{x}), \tag{4.1}$$

$$\alpha_{ij}^{x\to y} = \alpha_{ij}^{x} + z(\alpha_{ij}^{y} - \alpha_{ij}^{x}, \tag{4.2}$$

where the volume fraction of y-phase is expressed by a scalar variable z; $z = \eta$ for the R-phase transformation and $z = \xi$ for the M-phase transformation.

4.1. Transformation strain rate

The rate of the deviatoric transformation strain $\varepsilon_{ij}^{\mathrm{tr}(x\to y)}$ during the transformation from x-phase to y-phase is described by

$$\dot{\varepsilon}_{ij}^{\mathrm{tr}(x\to y)} = \Lambda_{ij}^{x\to y}\dot{z}, \tag{4.3}$$

http://rcin.org.pl

where the flow direction is characterized by the transformation tensor $\Lambda_{ij}^{x\to y}$ given by

$$\Lambda_{ij}^{x\to y} = \begin{cases} H^{*(x\to y)} N_{ij}^{\sigma}, & \dot{z} > 0, \\ H^{*(x\to y)} N_{ij}^{\varepsilon}, & \dot{z} < 0. \end{cases} \tag{4.4}$$

The coefficient $H^{*(x\to y)}$, which controls the magnitude of the transformation strain, is assumed to be

$$H^{*(x\to y)} = -\frac{\Gamma^{*(x\to y)}}{E^{x\to y}(z)} + \frac{E^y - E^x}{[E^{x\to y}(z)]^2}\sigma_e - (\alpha^y - \alpha^x)\Delta T, \tag{4.5}$$

where

$$\Gamma^{*(x\to y)} = \begin{cases} \Psi^*, & z = \eta, \\ \Omega^*, & z = \xi, \end{cases} \tag{4.6}$$

$$E^{x\to y}(z) = E^x + z(E^y - E^x). \tag{4.7}$$

In general, $\Gamma^{*(x\to y)}$ is a material function which depends on temperature and other internal variables. A simple temperature dependence is assumed in the simulations presented later. The basic constitutive relationship for TiNi SMAs is finally obtained as

$$\dot{\sigma}_{ij} = C_{ijkl}^{x\to y}(\dot{\varepsilon}_{kl} - \alpha_{kl}^{x\to y}\dot{T}) + Q_{ij}^{x\to y}\dot{z}, \tag{4.8}$$

where

$$Q_{ij}^{x\to y} = \left(C_{ijkl}^{y} - C_{ijkl}^{x}\right)\varepsilon_{kl}^{e} - C_{ijkl}^{x\to y}(\alpha_{kl}^{y} - \alpha_{kl}^{x})\Delta T - C_{ijkl}^{x\to y}\Lambda_{kl}^{x\to y}. \tag{4.9}$$

4.2. Transformation criteria

The transformation kinetics for TiNi SMAs was identified by LIN *et al.* [13] through uniaxial tensile tests using wire specimens. The uniaxial evolution equations determined for the volume fractions η and ξ of R-phase and M-phase can be written in a compact form using the representative volume fraction z as follows:

$$\dot{z} = (-1)^{\ell^{x\to y}} z^{m^{x\to y}} (1-z)^{n^{x\to y}} b^{x\to y}(c^{x\to y}\dot{T} - \dot{\sigma}). \tag{4.10}$$

The coefficients involved in this equation take different values for the forward and reverse transformations, and they are classified in Table 1 for the R-phase and M-phase transformations, respectively.

http://rcin.org.pl

Table 1. Coefficients involved in the evolution equations of phase volume fractions.

$x \to y$	z	$\ell^{x\to y}$	$m^{x\to y}$	$n^{x\to y}$	$b^{x\to y}$	$c^{x\to y}$
A→R	η	2	0	0	$b_{\mathrm{M}}^{\mathrm{R}}\dagger$	$c_{\mathrm{M}}^{\mathrm{R}}$
R→A	η	1	0	0	$b_{\mathrm{A}}^{\mathrm{R}}$	$c_{\mathrm{A}}^{\mathrm{R}}$
A→ M (R→M)	ξ	2	0	1	b_{M}	c_{M}
M→ A	ξ	1	1	0	b_{A}	c_{A}

$\dagger b_{\mathrm{M}}^{\mathrm{R}} = b_{\mathrm{M1}}^{\mathrm{R}}(T \le M_{\mathrm{S}}^{\mathrm{R}})$; $b_{\mathrm{M}}^{\mathrm{R}} = b_{\mathrm{M2}}^{\mathrm{R}}(T > M_{\mathrm{S}}^{\mathrm{R}})$

The evolution equation for the phase volume fraction is assumed to be rate-independent. The rate-independent formulation of the transformation kinetics for TiNi SMA was verified by WU *et al.* [44]. They elucidated that the effect of the loading rate on the stress-strain relationships for SMAs were caused by the temperature variation due to the latent heat. Suppressing the change in temperature, the stress-strain behaviour observed for different strain rates almost agreed with each other. This reveals that the transformation mechanisms of SMAs are essentially rate-independent.

The uniaxial transformation start and finish conditions for TiNi SMA were also determined by LIN *et al.* [13]. Under uniaxial tensile loading conditions, the transformation start and finish stresses of R-phase at a low temperature are almost constant, while at a higher temperature they increase in proportion to temperature. Therefore, the transformation lines (TL) on the stress-temperature plane which characterize the transformation start/finish conditions of R-phase were described using two-segment parallel broken lines. Namely, the transformation line (TL) for the R-phase transformation on the stress-temperature plane is composed of two intersecting straight lines: a horizontal line (TL_1) and another line (TL_2) extending in the right upper direction. For the R-phase transformation, it should be noticed that the temperatures at the intersections of the segment lines do not coincide with the stress-free transformation start/finish temperatures. For the M-phase transformation, on the other hand, the relationships between the transformation start/finish stresses and temperature can be described by straight lines. Similar to Eq. (4.10), the relationships between the transformation start/finish stresses and temperature can be written as

$$\sigma^{Y} = d^{x\to y}(T - T^{x\to y}) - \sigma^{(0)}, \tag{4.11}$$

where the superscript Y represents the label of start or finish. The coefficients involved depend on the transformation conditions, and they are classified as

http://rcin.org.pl

shown in Table 2. In Table 2, the forward and reverse transformation lines are symbolically expressed by $\mathrm{TL(M^R)}$ and $\mathrm{TL(A^R)}$ for the R-phase transformation and by TL(M) and TL(A) for the M-phase transformation, respectively.

Table 2. Transformation start and finish streses.

$x \to y$	TL	Y	z	$d^{x\to y}$	$T^{x\to y}$	$\sigma^{(0)}$
A→R	$\mathrm{TL_1(M^R)}$	start	η	0	–	$-\sigma^{\mathrm{R}}_{\mathrm{MO}}$
		finish		0	–	$-\sigma^{\mathrm{R}}_{\mathrm{MO}} + 1/b^{\mathrm{R}}_{\mathrm{M1}}$
	$\mathrm{TL_2(M^R)}$	start		$c^{\mathrm{R}}_{\mathrm{M}}$	$M^{\mathrm{R}}_{\mathrm{S}}$	0
		finish		$c^{\mathrm{R}}_{\mathrm{M}}$	$\mathrm{M^R_S}$	$1/b^{\mathrm{R}}_{\mathrm{M2}}$
R→A	$\mathrm{TL_1(A^R)}$	start		0	–	$-\sigma^{\mathrm{R}}_{\mathrm{AO}}$
		finish		0	–	$-\sigma^{\mathrm{R}}_{\mathrm{AO}} + 1/b^{\mathrm{R}}_{\mathrm{A}}$
	$\mathrm{TL_2(A^R)}$	start		$c^{\mathrm{R}}_{\mathrm{A}}$	$\mathrm{A^R_S}$	0
		finish		$c^{\mathrm{R}}_{\mathrm{A}}$	$\mathrm{A^R_S}$	$1/b^{\mathrm{R}}_{\mathrm{A}}$
A→ M	TL(M)	start	ξ	c_{M}	$\mathrm{M_S}$	0
		finish		c_{M}	$\mathrm{M_S}$	$2\ln(10)/b_{\mathrm{M}}$
M→ A	TL(A)	start		c_{A}	$\mathrm{A_S}$	0
		finish		c_{A}	$\mathrm{A_S}$	$2\ln(10/b_{\mathrm{A}}$

For analyses of the transformation behaviour of TiNi SMA in the present study, simple multiaxial extensions of the uniaxial evolution equation for the phase volume fraction and of the transformation start and finish stresses are assumed; viz., the uniaxial stress and stress rate are replaced with the von Mises equivalent stress and its time rate, respectively.

4.3. Limitations

For the TiNi SMA examined by LIN *et al.* [13], the uniaxial transformation finish stresses of R-phase and M-phase are negative in the temperature range where the shape memory effect is observed. Thus, the multiaxial transformation kinetics of J_2 type discussed in the present study can be used only for analyses of the pseudoelastic behaviour. Moreover, the J_2-type extension excludes consideration for the tension-compression asymmetry of the pseudoelastic behaviour [45, 46], the volumetric change due to phase transformation [47], the pressure dependence of the transformation kinetics [48 – 50] and the rubber-like behaviour due to reorientation [51].

http://rcin.org.pl

The pseudoelastic transformation of TiNi SMA is incrementally evaluated by integrating the rate evolution equation of the phase volume fraction: Eq. (4.10). For given rates (or increments) of stress and temperature, the current sign of the rate of volume fraction and the current stress and temperature on the phase transformation diagram characterized by the transformation start and finish lines enable us to evaluate numerically what kind of phase transformation follows. Using the incremental calculations based on the stress-temperature diagram, it is possible to know if the next incremental step corresponds to the transformation loading or unloading. For a neutral thermomechanical loading along the phase transformation line, no phase transformation proceeds in the present modelling. The validity of this assumption should be examined in future studies. It is also an interesting subject to model the consecutive R-phase and M-phase transformations of TiNi SMA on the basis of more sophisticated multiaxial criteria for the transformation loading-unloading and descriptions of the transformation potential surfaces [28 – 29].

5. Numerical simulations

5.1. Material constants

The material constants to characterize the R-phase and M-phase transformation kinetics for TiNi SMAs are listed in Table 3 and Table 4. These data were taken from the experimental study performed by LIN *et al.* [13]. Since the elastic moduli of the monolithic R-phase and M-phase were not found in literature, they were assumed as listed in Table 5.

Table 3. Material constants for the R-phase transformation of TiNi.

b^{R}_{M1} MPa^{-1}	b^{R}_{M2} MPa^{-1}	c^{R}_{M} $MPaK^{-1}$	b^{R}_{A} $MPaK^{-1}$	c^{R}_{A} $MPaK^{-1}$	M^{R}_{S} K	A^{R}_{S} K	σ^{R}_{M0} MPa	σ^{R}_{A0} MPa
−0.094	−0.028	15.2	0.025	17.4	317.0	318.0	25	5

Table 4. Material constants for the M-phase transformation of TiNi.

b^{M} MPa^{-1}	c^{M} $MPaK^{-1}$	b^{A} MPa^{-1}	c^{A} $MPaK^{-1}$	M_S K	A_S K
−0.132	6.125	0.132	8.8	272.5	318

Table 5. Mechanical properties of TiNi.

α^{M} K^{-1}	α^{R} K^{-1}	α^{A} K^{-1}	ν	E^{A} MPa	E^{M} MPa	E^{R} MPa
6.6E-06	6.6E-06	11.0E-06	0.33	80.0E+03	30.0E+03	80.0E+03

http://rcin.org.pl

The parameter $\Gamma^{*(x\to y)}$ controlling the transformation strain range was assumed to be a function of only temperature in the range (300 ~ 360 K) examined by LIN *et al.* [13]. On the basis of the stress-strain relationships for TiNi SMAs [13], the material function was determined as

$$\Psi^* = 6.49T - 2286, \tag{5.1}$$

for the R-phase transformation, and

$$\Omega^* = -6.0T - 700, \tag{5.2}$$

for the M-phase transformation. The unit of Ψ^* and Ω^* is MPa/K.

5.2. Results of uniaxial simulations

First of all, we have performed the numerical simulations which correspond to the experimental results reported by LIN *et al.* [13].

Figure 1(a) shows the predicted stress-strain behaviour of TiNi SMAs at 303 K for a single loading-unloading cycle in tension ($\sigma_{\max} = 200$ MPa). We can clearly observe two phenomena: 1) at 303 K both the R-phase and M-phase transformations occur, and 2) the strain is not entirely recovered by complete unloading. Fig. 1(b) shows the similar result at 303 K when loaded up to a larger stress $\sigma_{\max} = 700$ MPa. In this case, the initial loading was given until the M-phase transformation was completely finished. It is important to read from the first observation that the R-phase transformation varies the appearance of the overall stress-strain behaviour. The second phenomenon indicates that the shape memory effect appears at 303 K and the residual strain is recovered by heating.

Figures 2(a) through 2(c) show the predicted stress-strain curves at 333 K for loading up to different maximum tensile stresses ($\sigma_{\max} = 370$, 372 and 700 MPa). The total strain completely recovers with unloading, irrespective of the value of the prior maximum tensile stress. Hence, the TiNi SMA at 333 K exhibits the pseudoelastic behaviour. More detailed observations are made as follows. A small pseudoelastic hysteresis loop shown in Fig. 2(a) is caused by the R-phase transformation. In Fig. 2(b), we can see that the R-phase and M-phase transformations take place. Note that the TiNi SMA is unloaded before the M-phase transformation is completely finished. During unloading, therefore, the residual R-phase first transforms back to A-phase, and then the M-phase induced by the prior loading changes to A-phase. In the numerical simulation shown in Fig. 2(c), the M-phase transformation is completed during the prior tensile loading. Thus, the subsequent unloading behaviour is characterized by the elastic unloading and the reverse transformation of M-phase.

http://rcin.org.pl

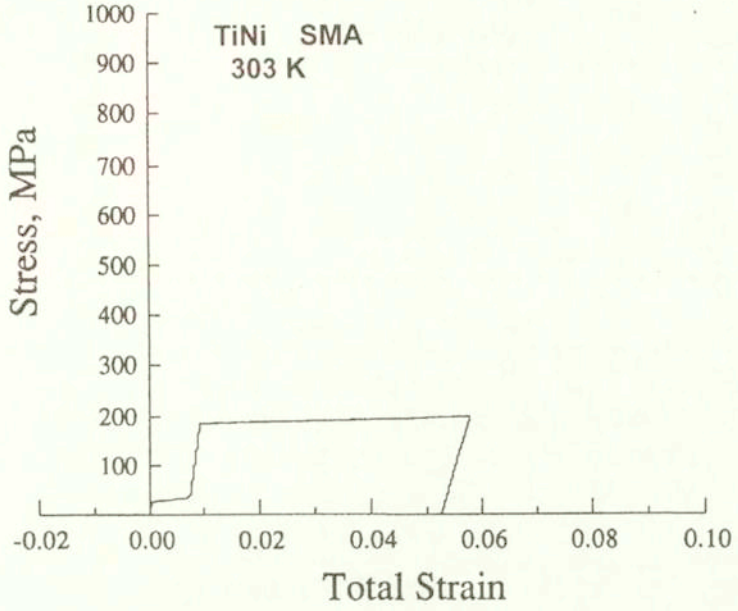

(a) $\sigma_{max} = 200$ MPa

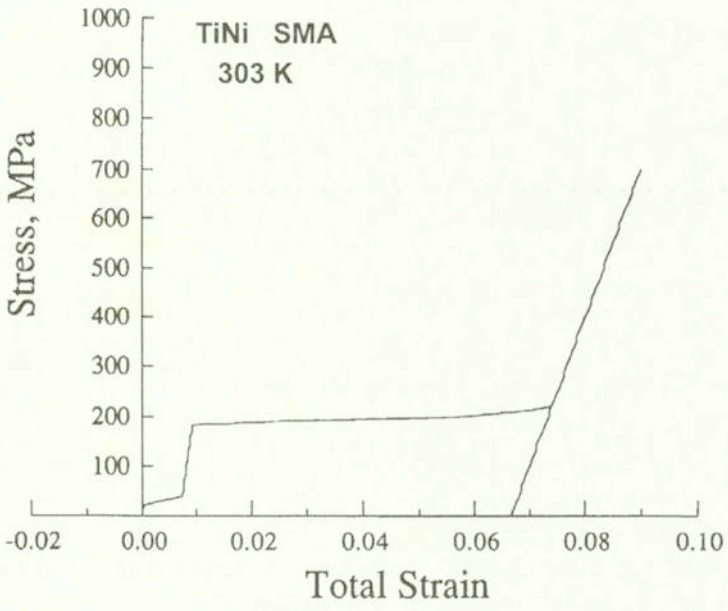

(b) $\sigma_{max} = 700$ MPa

FIG. 1. Predicted uniaxial stress-strain curve for TiNi-SMA at 303 K. (a) $\sigma_{max} = 200$ MPa; (b) $\sigma_{max} = 700$ MPa.

http://rcin.org.pl

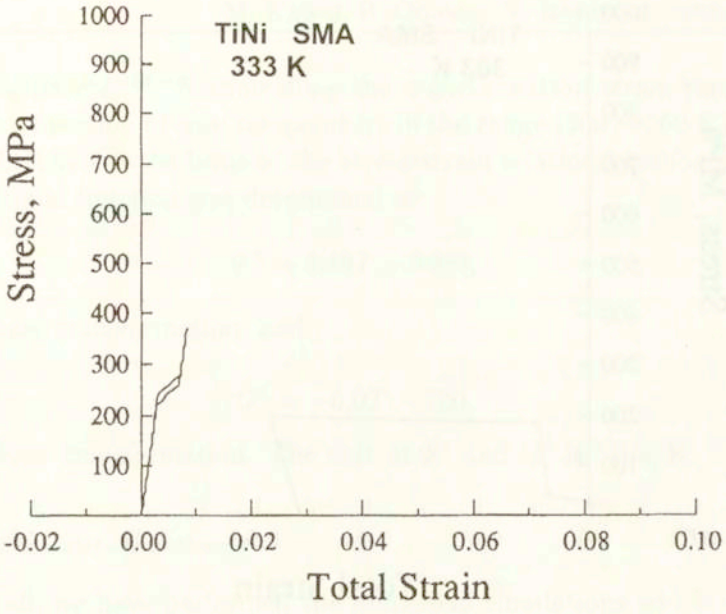

(a) $\sigma_{max} = 370$ MPa

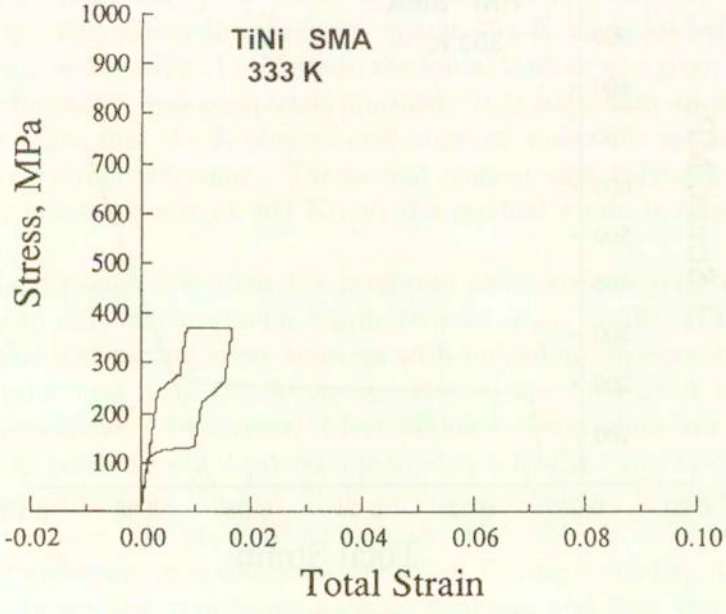

(b) $\sigma_{max} = 372$ MPa

[FIG. 2(a),(b)]

http://rcin.org.pl

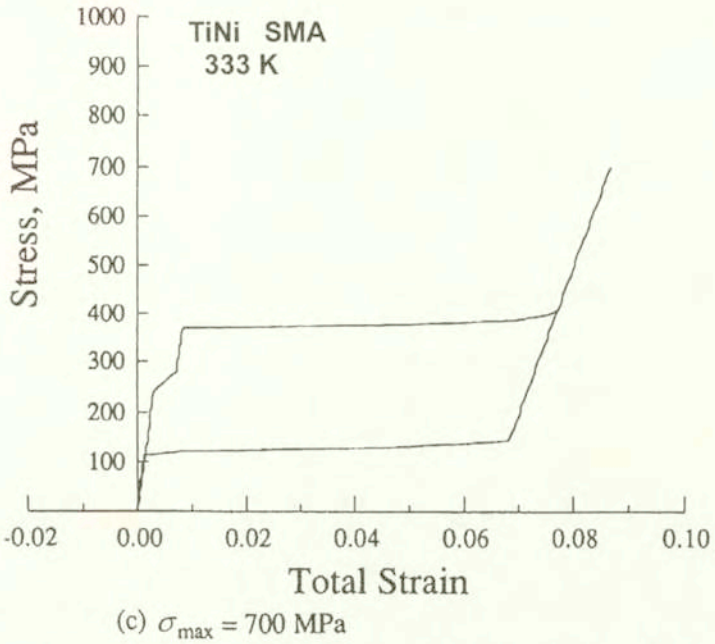

FIG. 2. Predicted uniaxial stress-strain curve for TiNi-SMA at 333 K. (a) σ_{max} = 370 MPa; (b) σ_{max} = 372 MPa; (c) σ_{max} = 700 MPa.

Figures 3(a) through 3(c) show the predicted stress-strain relationships for loading-unloading cycles at 353 K (σ_{max} = 495, 500 and 700 MPa). Also at 353 K, the transformation strain completely recovers with unloading. Hence, the predicted behaviour is pseudoelastic. Unlike the previous simulations shown in Figs. 2(a) through 2(c), the R-phase transformation does not appear at 353 K and the pseudoelastic behaviour is caused only by the M-phase transformation.

The predictions using the present constitutive model obviously differ from those using the SMA models which describe only the M-phase transformation. Namely, as observed in Figs. 1 and 2, the stress-strain behaviour of TiNi SMAs is significantly influenced by the R-phase transformation. To evaluate the PE and SME of TiNi SMAs in such a low stress regime, a capability to predict the R-phase transformation is required in the SMA model assumed. This partly proves the significance of the proposed constitutive model for TiNi SMA.

The SMA constitutive model used for these simulations takes into account the change in stiffness due to phase transformation. Therefore, the slopes of the stress-strain relationships during elastic unloading vary depending on the extent of the forward transformation. For example, a difference between the Young's moduli of A-phase and M-phase can be observed in Fig. 3(c). In the Tanaka model, a constant average stiffness is assumed for the whole process of the phase transformation, and the effect of stiffness change caused by the phase transfor-

http://rcin.org.pl

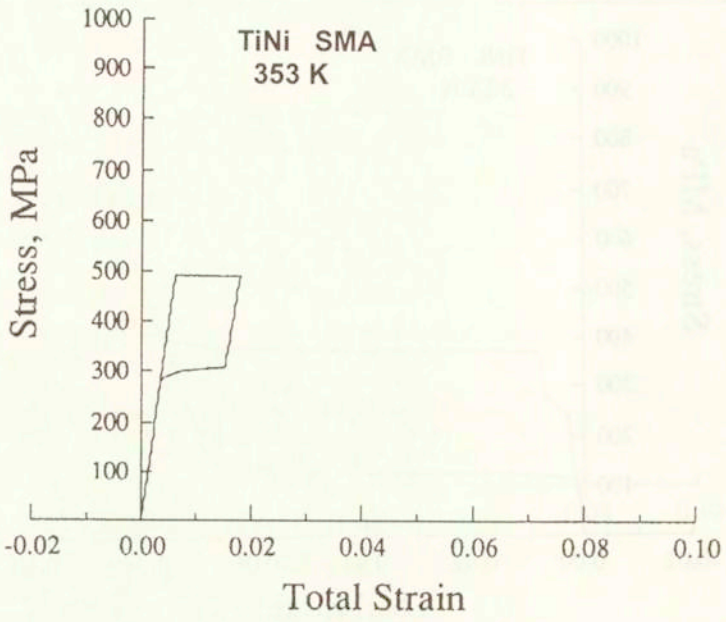

(a) $\sigma_{max} = 495$ MPa

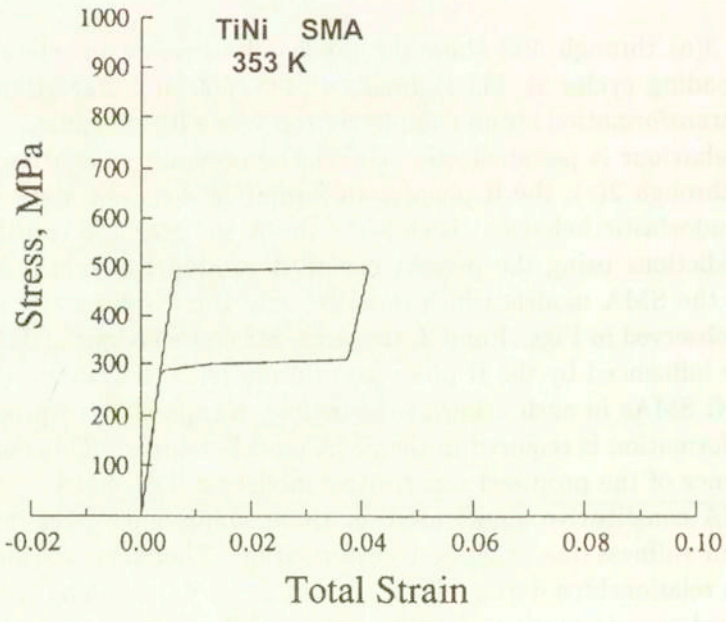

(b) $\sigma_{max} = 500$ MPa

[FIG. 3(a), (b)]

http://rcin.org.pl

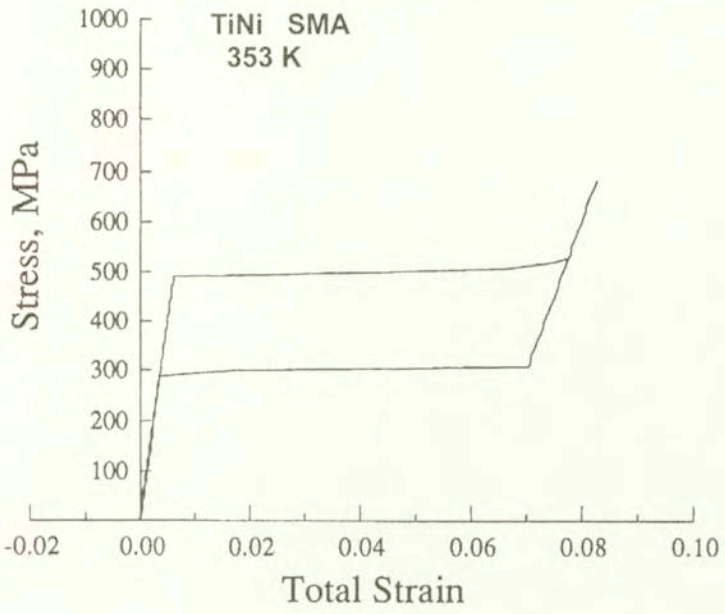

FIG. 3. Predicted uniaxial stress-strain curve for TiNi-SMA at 353 K. (a) σ_{max} = 495 MPa; (b) σ_{max} = 500 MPa; (c) σ_{max} = 700 MPa.

mation is not described. However, the uniaxial simulations presented above do not differ much from those predicted by using the uniaxial Tanaka model. This means that these simulation results are in good agreement with the experimental results reported by LIN *et al.* [13]. As far as the present simple loading conditions are concerned, therefore, a consideration of the transformation-induced stiffness change does not drastically alter the appearance of the pseudoelastic stress-strain behaviour.

5.3. Results of multiaxial simulations

To observe the multiaxial transformation behaviour of TiNi SMAs predicted by the present SMA model, the pseudoelastic behaviour under combined tension and torsion and biaxial tension was simulated at a constant temperature of 333 K.

Figures 4 and 5 show the predicted axial and torsional stress-strain curves for multiaxial proportional loading-unloading cycles under combined tension and torsion. On the plane $(\sigma_{11}, \sqrt{3}\sigma_{12})$, the stress is applied along the line paths with slopes of $\theta = \text{arctg}(\sqrt{3}\sigma_{12}/\sigma_{11}) = 30°$ and 45°, respectively. Since the present SMA model assumes the transformation plasticity based on the von Mises equivalent stress, the tensile and torsional phase transformations simultaneously

http://rcin.org.pl

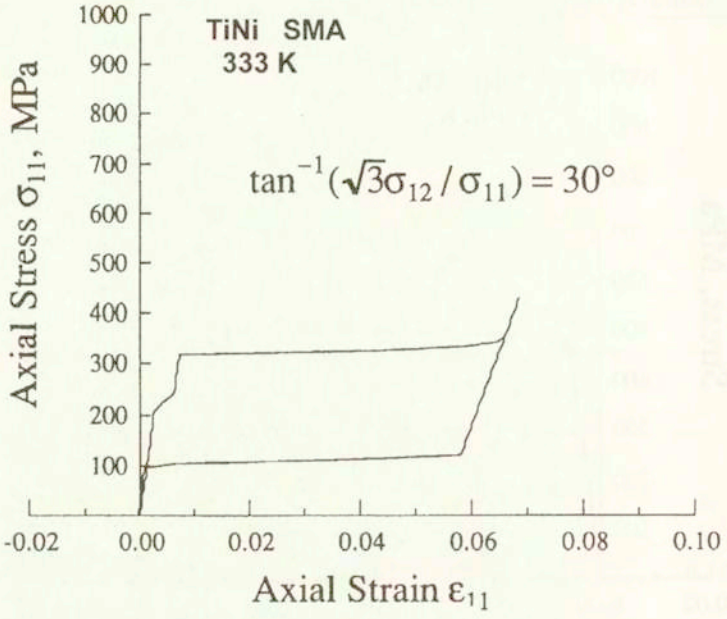

(a) Axial stress-strain curve

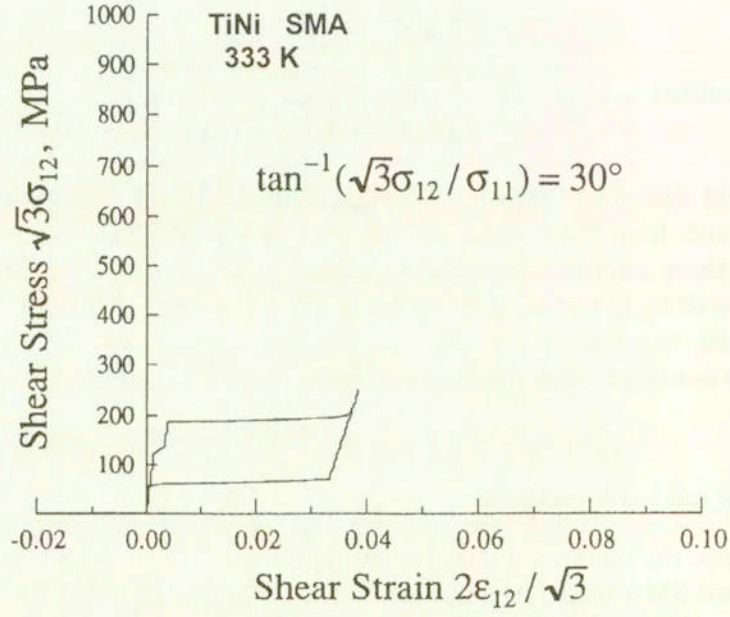

(b) Torsional stress-strain curve

FIG. 4. Predicted stress-strain curves for TiNi-SMA at 333 K under tension-torsion proportional loading (arc $\mathrm{tg}(\sqrt{3}\sigma_{12}/\sigma_{11}) = 30°$). (a) Axial stress-strain curve; (b) Torsional stress-strain curve.

http://rcin.org.pl

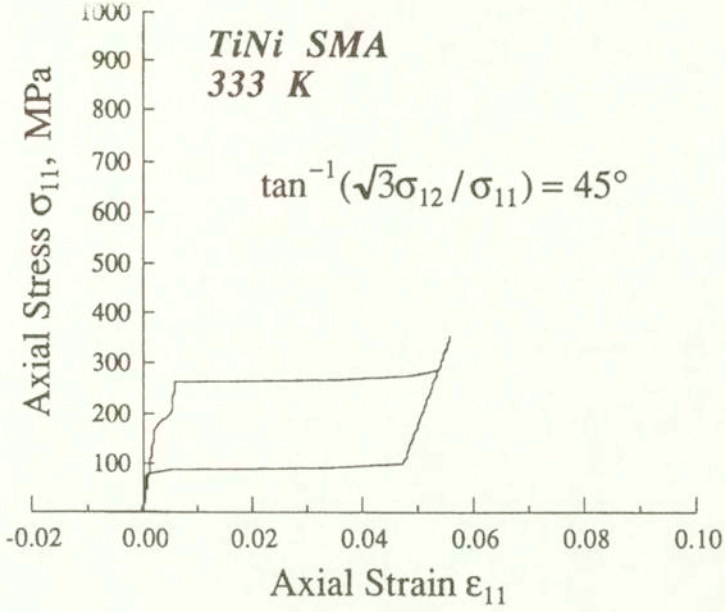

(a) Axial stress-strain curve

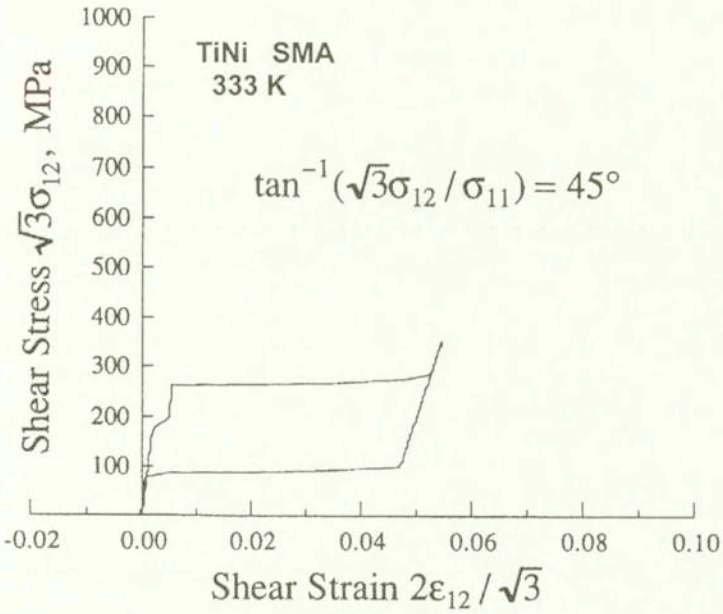

(b) Torsional stress-strain curve

FIG. 5. Predicted stress-strain curves for TiNi-SMA at 333 K under tension-torsion proportional loading (arc $\mathrm{tg}(\sqrt{3}\sigma_{12}/\sigma_{11}) = 45°$). (a) Axial stress-strain curve; (b) Torsional stress-strain curve.

http://rcin.org.pl

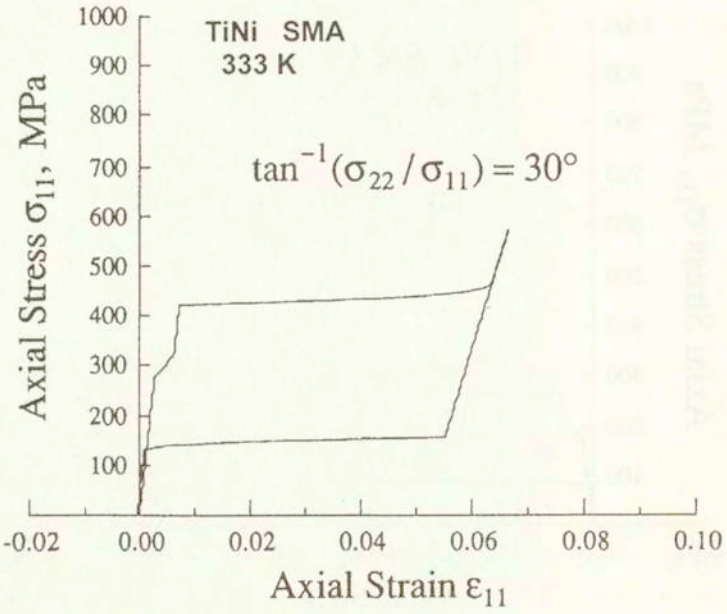

(a) σ_{11} v.s. ε_{11}

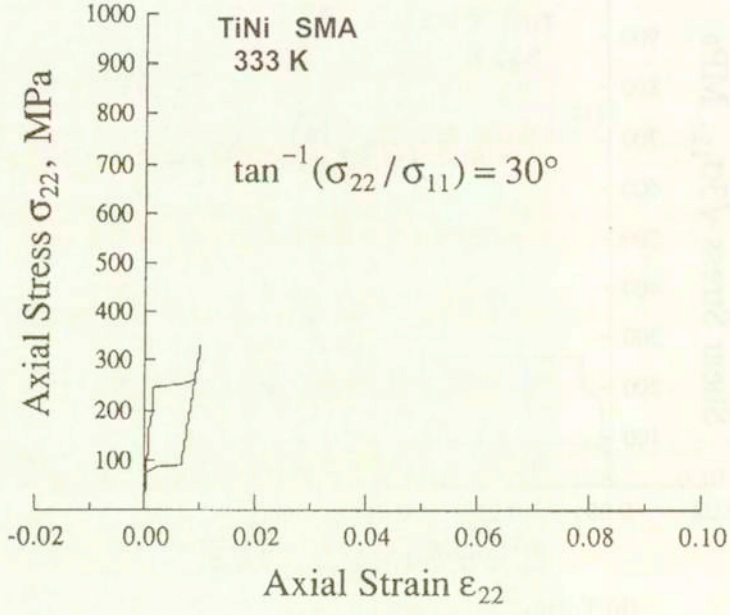

(b) σ_{22} v s. ε_{22}

FIG. 6. Predicted stress-strain curves for TiNi-SMA at 333 K under biaxial proportional loading (arc tg$(\sigma_{22}/\sigma_{11}) = 30°$). (a) σ_{11} vs. ε_{11}; (b) σ_{22} vs. ε_{22}.

http://rcin.org.pl

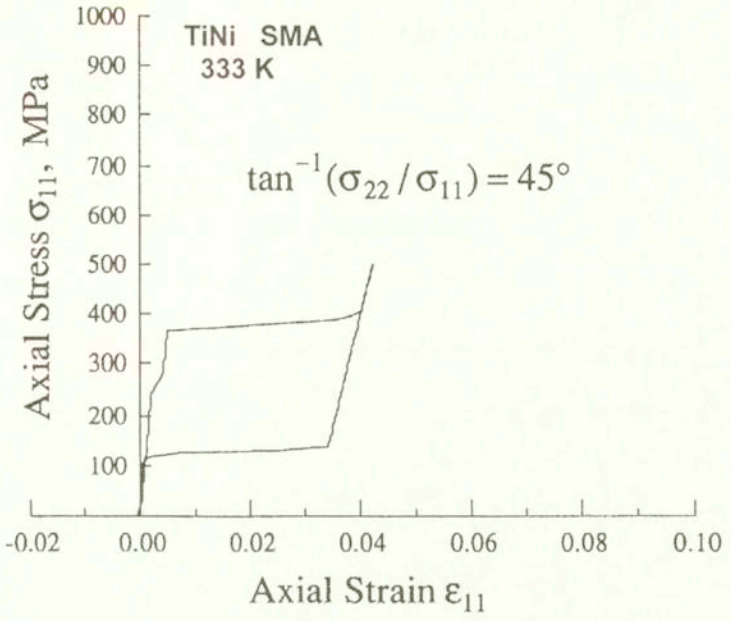

(a) σ_{11} v.s. ε_{11}

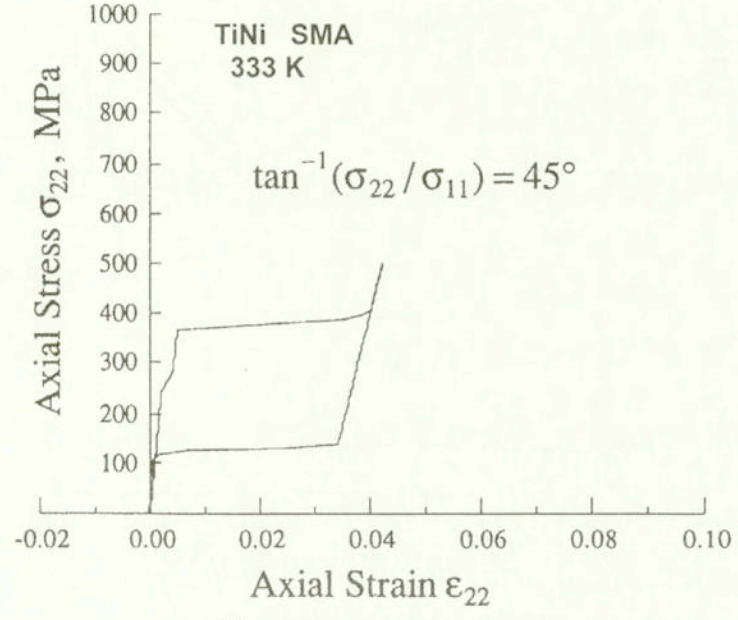

(b) σ_{22} v s. ε_{22}

FIG. 7. Predicted stress-strain curves for TiNi-SMA at 333 K under biaxial proportional loading (arc $\mathrm{tg}(\sigma_{22}/\sigma_{11}) = 45°$). (a) σ_{11} vs. ε_{11}; (b) σ_{22} vs. ε_{22}.

http://rcin.org.pl

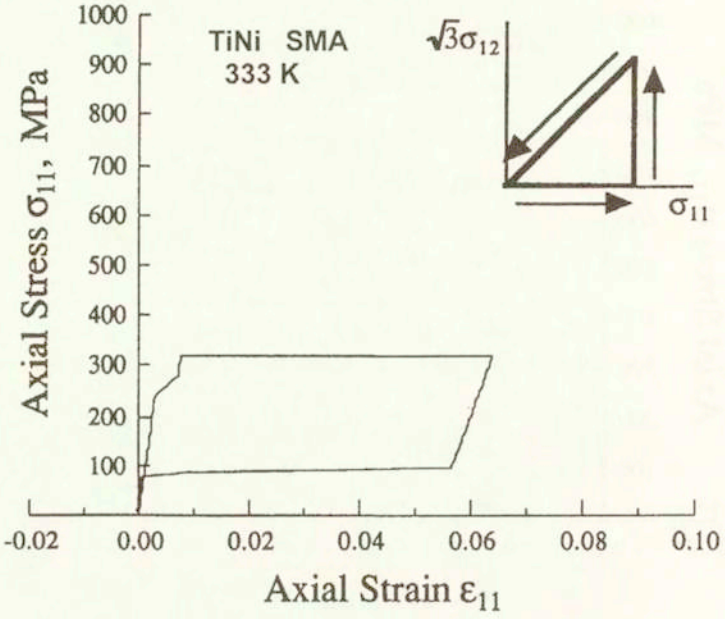

(a) Axial stress-strain curve

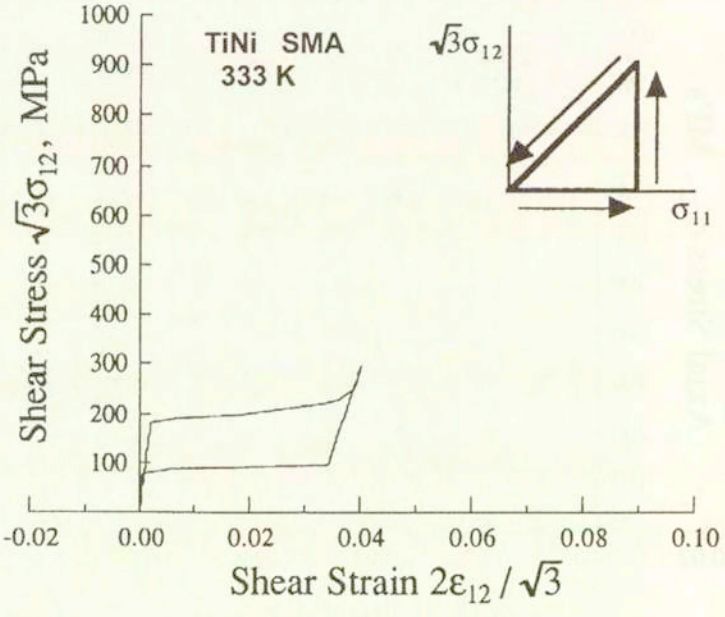

(b) Torsional stress-strain curve

FIG. 8. Predicted stress-strain curves for TiNi-SMA at 333 K under tension-torsion nonproportional loading; (a) Axial stress-strain curve; (b) Torsional stress-strain curve.

http://rcin.org.pl

continue, once the transformation condition is satisfied. It is important to note that the transformation strain ranges in the component stress-strain relationships differ, depending on the magnitude of the component stresses. Namely, an identical stress-strain curve is predicted in tensile and torsional directions for the case of $\theta = 45°$, while for $\theta = 30°$ the stress-strain curve and the maximum transformation strain in the torsion component become smaller than those in the tensile component.

Figures 6 and 7 present the predicted stress-strain behaviour under biaxial tension for $\theta = \text{arctg}(\sigma_{22}/\sigma_{11}) = 30°$ and 45°, respectively. These results are similar to those for combined tension and torsion.

The SMA behaviour predicted for a multiaxial nonproportional loading and unloading path under combined tension and torsion is shown in Fig. 8. Unlike the simulations discussed above for proportional loading paths, the torsional stress-strain relationship does not exhibit the R-phase transformation. This is because the R-phase transformation is entirely finished during the prior tensile loading. If the nonproportional stress path is changed so that the torsion comes first, the results become opposite and the R-phase transformation in turn appears only in the torsional stress-strain relationship. Under the multiaxial nonproportional loading conditions, therefore, the phase transformation behaviour of TiNi SMAs becomes much more complicated due to such a path-dependence.

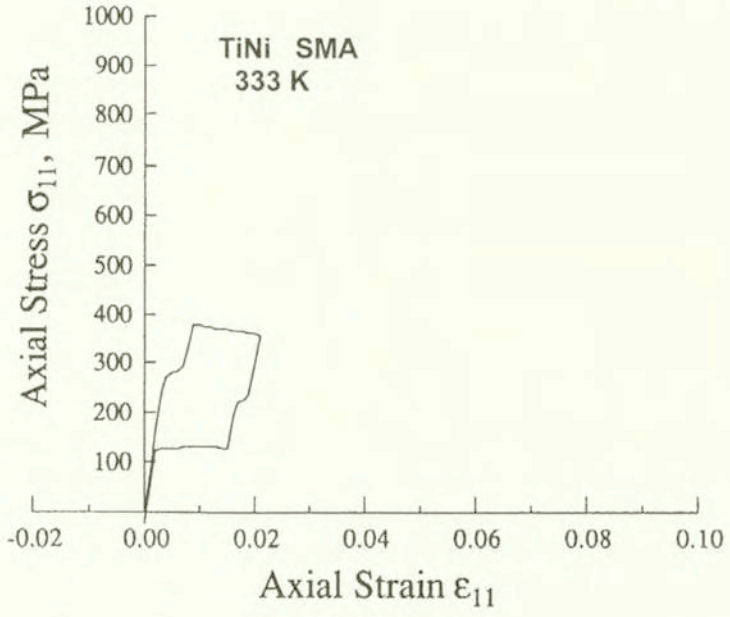

(a) $\varepsilon_{11\max} = 0.02$

[FIG. 9(a)]

http://rcin.org.pl

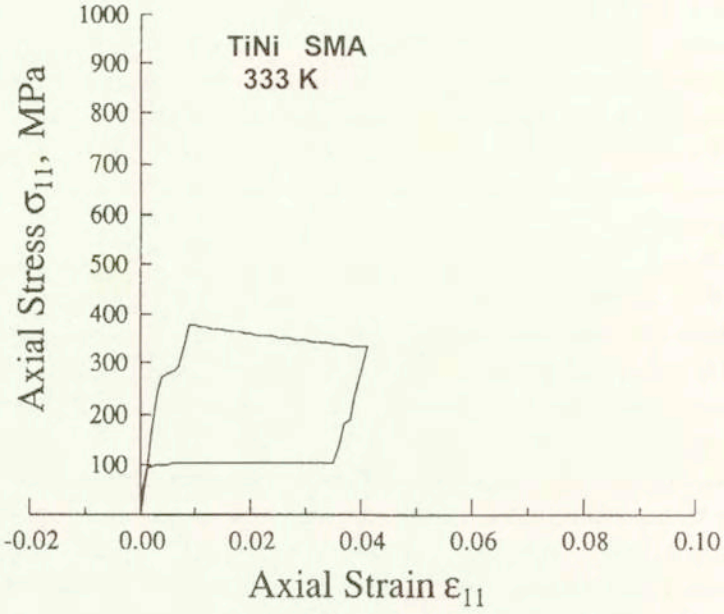

FIG. 9. Predicted stress-strain curves for TiNi-SMA at 333 K under tensile straining (arc tg$(2\varepsilon_{12}/\sqrt{3}/\varepsilon_{11}) = 0°$). (a) $\varepsilon_{11\,max} = 0.02$; (b) $\varepsilon_{11\,max} = 0.04$.

Finally, the predicted stress-strain relationships in the loading direction for a strain-controlled uniaxial tension are presented in Figs. 9(a) and 9(b). Since the lateral contraction is constrained, TiNi SMA is simultaneously subjected to tensile stresses in the lateral directions. Therefore, these results also demonstrate the multiaxial transformation behaviour of TiNi SMAs.

6. Conclusion

A three-dimensional phenomenological constitutive model for describing the transformation behaviour of TiNi shape memory alloys was developed with a particular emphasis on an incorporation of the R-phase and M-phase transformations into a multiaxial formulation. An expression of the transformation strain range was proposed which was influenced by the applied stress and the current phase volume fraction. The three-dimensional model presented may be classified as an extension of the uniaxial Tanaka model and the multiaxial Boyd-Lagoudas model. The proposed model can reproduce fairly well the observed stress-strain behaviour of TiNi SMAs under uniaxial loading conditions. The capability of the

http://rcin.org.pl

proposed model to describe the pseudoelastic behaviour under several isothermal multiaxial proportional and nonproportional loading conditions, is also elucidated through numerical simulations. From these numerical simulations, it is verified that the proposed expression of the transformation strain range is effective to predict the closed hysteresis loops under various pseudoelastic loading conditions.

It was thus demonstrated that the multiaxial constitutive model developed to describe the R-phase and M-phase transformations of TiNi SMAs could be used as a tool for analysis-based designs of SMA composites and structures. However, some important phenomena, e.g., the volumetric change due to phase transformation, the pressure dependence of the transformation kinetics and the rubber-like behaviour caused by a reorientation, were disregarded in the present study. Therefore, an appropriate incorporation of capabilities to describe these phenomena into modelling, together with a verification based on multiaxial experiments, should be made in the future research.

References

1. M.V. GANDHI and B.S. THOMPSON, *Smart materials and structures*, 192–215, Chapman and Hall, 1992.
2. B. CULSHAW, *Smart structures and materials*, 122–126, Artech House, 1996.
3. T. TAKAGI, *Recent research on intelligent materials*, [in:] Proc. Int. Symp. on Microsystems, Intelligent Materials and Robots, 3–10, 1995.
4. C.A. ROGERS and Z. CHAUDHRY, *Smart structures: on-line monitoring concepts and challenges*, Proc. [in:] Int. Symp. on Microsystems, Intelligent Materials and Robots, 407–410, 1995.
5. A. BAZ, S. POH, J. RO, M. MUTUA and J. GILHEANY, *Active control of nitinol-reinforced composite beam*, [in:] Intelligent Structural Systems, H.S. Tzou and G.L. Anderson [Eds.], 169–212, 1992.
6. K. OTSUKA, *Fundamentals of shape memory alloys – in view of intelligent materials*, [in:] Proc. Int. Symp. on Microsystems, Intelligent Materials and Robots, 225–230, 1995.
7. C. LIANG and C.A. ROGERS, *Design of shape memory alloy springs with applications in vibration control*, ASME Journal of Vibration and Acoustics, **115**, 129–135, 1993.
8. P.F. GOBIN, G. GUENIN, M. MORIN and J. TATIBOUET, *Smart materials: a future for composites*, [in:] Proc. Int. Symp. on Microsystems, Intelligent Materials and Robots, 239–242, 1995.
9. K. TANAKA, *A thermomechanical sketch of shape memory effect: one-dimensional tensile behavior*, Res Mechanica, **18**, 251–263, 1986.
10. K. TANAKA, S. KOBAYASHI and Y. SATO, *Thermomechanics of transformation pseudoelasticity and shape memory effect in alloys*, International J. Plasticity, **2**, 59–72, 1986.
11. K. TANAKA, *A phenomenological description on thermomechanical behavior of shape memory alloys*, [in:] Elastic-Plastic Failure Modelling of Structures With Applications, D. Hui and T.J. Kozik [Eds.], PVP **141**, 163–170, 1988.

http://rcin.org.pl

12. K. TANAKA and Y. SATO, *Phenomenological description on mechanical behavior of shape memory alloys*, Trans. JSME, **53**, 491, 1368–1373, 1992.

13. P. LIN, H. TOBUSHI, K. TANAKA, T. HATTORI and K. UCHINO, *Deformation properties associated with martensitic and R-phase transformation in TiNi shape memory alloy*, Trans. JSME, **60**, 569, A, 126–133, 1994.

14. H. TOBUSHI, K. TANAKA, T. HORI, T. SAWADA and T. HATTORI, *Pseudoelasticity of TiNi shape memory alloy (Dependence on maximum strain and temperature)*, Trans. JSME, **58**, 549, A, 694–699, 1992.

15. H. TOBUSHI, H. IWANAGA, A. INABA and M. KAWAGUCHI, *A study on mechanical properties of TiNi shape memory alloy (Experiments on cyclic characteristics of shape memory effect)*, Trans. JSME, **55**, 515, A, 1663–1668, 1989.

16. A. INABA, K. KIMURA, H. IWANAGA and H. TOBUSHI, *A study on mechanical properties of TiNi shape memory alloy (Experiments on cyclic characteristics of pseudo-elasticity)*, Trans. JSME, **55**, 511, A, 628–633, 1989.

17. C. LIANG and C.A. ROGERS, *One-dimensional thermomechanical constitutive relations for shape memory materials*, Journal of Intelligent Material Systems and Structures, **1**, 2, 207–234, 1990.

18. L.C. BRINSON, *One-dimensional constitutive behavior of shape memory alloys: thermomechanical derivation with non-constant material functions*, Journal Intelligent Material Systems and Structures, **4**, 2, 229–242, 1993.

19. I. MÜLLER and H. XU, *On the pseudo-elastic hysteresis*, Acta Metall. Mater., **39**, 3, 263–271, 1991.

20. E.J. GRAESSER and F.A. COZZARELLI, *Shape-memory alloys as new materials for aseismic isolation*, ASCE, Journal of Engineering Mechanics, **117**, 11, 2590–2608, 1991.

21. Y. IVSHIN and T.J. PENCE, *A constitutive model for hysteretic phase transition behavior*, Int. J. Eng. Sci., **32**, 681–704, 1994.

22. Y. IVSHIN and T.J. PENCE, *A thermodynamical model for a one-variant shape memory material*, Journal of Intelligent Material Systems and Structures, **5**, 455–473, 1994.

23. R. ABEYARATNE, S.J. KIM and J.K. KNOWLES, *A one-dimensional continuum model for shape-memory alloys*, Int. J. Solids and Structures, **31**, 16, 2229–2249, 1994.

24. D.J. BARRETT, *A one-dimensional constitutive model for shape memory alloys*, Journal of Intelligent Material Systems and Structures, **6**, 329–337, 1995.

25. C. LIANG and C.A. ROGERS, *The multi-dimensional constitutive relations of shape memory alloys*, [in:] Proceedings of the AIAA 32nd Structures, Conf. Structural Dynamics and Materials Conference, 178–185, 1991.

26. J.G. BOYD and D.C. LAGOUDAS, *Thermomechanical response of shape memory composites*, Journal of Intelligent Material Systems and Structures, **5**, 333–346, 1994.

27. D.C. LAGOUDAS, J.G. BOYD and Z. BO, *Micromechanics of active composites with SMA fibers*, Journal of Engineering Materials and Technology, **116**, 337–347, 1994.

28. B. RANIECKI, CH. LEXCELLENT and K. TANAKA, *Thermodynamic models of pseudoelastic behaviour of shape memory alloys*, Arch. Mech., **44**, 3, 261–288, 1992.

29. B. RANIECKI and C. LEXCELLENT, *R_L-models of pseudoelasticity and their specification for some shape memory solids*, Eur. J. Mech., A/Solids, **13**, 1, 21–50, 1994.

http://rcin.org.pl

30. C. ROGUEDA, C. LEXCELLENT and L. BOCHER, *Experimental study of pseudoelastic behaviour of a CuZnAl polycrystalline shape memory alloy under tension-torsion proportional and non-proportional loading tests*, Arch. Mech., **48**, 6, 1025–1045, 1996.

31. E.J. GRAESSER and F.A. COZZARELLI, *A proposed three-dimensional constitutive model for shape memory alloys*, Journal of Intelligent Material Systems and Structures, **5**, 78–89, 1994.

32. L.C. BRINSON and S. HWANG, *Simplifications and comparisons of shape memory alloy constitutive models*, Journal of Intelligent Material Systems and Structures, **7**, 97–107, 1996.

33. E. PATOOR, A. EBERHARDT and M. BERVEILLER, *Thermodynamic behaviour of shape memory alloys*, Arch. Mech., **40**, 5–6, 775–794, 1988.

34. E. PATOOR, A. EBERHARDT and M. BERVEILLER, *Micromechanical modelling of superelasticity in shape memory alloy*, J. de Physique IV, C1, **6**, 277–292, 1996.

35. Q.P. SUN and K.C. HWANG, *Micromechanics modelling for the constitutive behavior of polycrystalline shape memory alloy -I. Derivation of general relations*, Journal of the Mechanics and Physics of Solids, **41**, 1, 1–17, 1993.

36. Q.P. SUN and K.C. HWANG, *Micromechanics modelling for the constitutive behavior of polycrystalline shape memory alloy -II. Study of the individual phenomena*, Journal of the Mechanics and Physics of Solids, **41**, 1, 19–33, 1993.

37. F.D. FISCHER, Q.P. SUN and K. TANAKA, *Transformation-induced plasticity (TRIP)*, Applied Mechanics Reviews, **49**, 6, 317–364, 1996.

38. V. BIRMAN, *Review of mechanics of shape memory alloy structures*, Applied Mechanics Reviews, **50**, 11, 629–645, 1997.

39. M. TOKUDA and P. SITTNER, *Polycrystalline shape memory alloy under multi-axial loading conditions*, J. Soc. Mat. Sci., **45**, 5, 527–536, 1996.

40. P. SITTNER, M. TAKAKURA, Y. HARA and M. TOKUDA, *On transformation pathways of general stress controlled thermoelastic martensitic transformation in shape memory alloys*, J. de Physique IV, C1, **6**, 357–366, 1996.

41. H. FUNAKUBO [Ed.], *Shape memory alloys*, New York, Gordon and Breach Science Publishers, 1987.

42. K. TANAKA, H. TOBUSHI and S. MIYAZAKI, *Mechanical properties of shape memory alloys* (in Japanese), Yokendo, 1993.

43. L.C. MAGEE, *Phase transformation*, H. I. Aaronson [Ed.], 115, AMS, 1969.

44. K. WU, F. YANG, Z. PU and J. SHI, *The effect of strain rate on detwinning and superelastic behavior of NiTi shape memory alloys*, Journal of Intelligent Material Systems and Structures, **7**, 138–144, 1996.

45. P. SITTNER, V. NOVAK and N. ZARUBOVA, *Martensitic transformations in [001] CuAlZnMn single crystals*, Acta Mater., **46**, 4, 1265–1281, 1998.

46. Y. LIU, Z. XIE, J.V. HUMBEECK and L. DELAEY, *asymmetry of stress-strain curves under tension and compression for NiTi shape memory alloys*, Acta mater., **46**, 12, 4325–4338, 1998.

47. K. JACOBUS, H. SEHITOGLU and M. BALZER, *Effect of stress state on the stress-induced martensitic transformation in polycrystalline Ni-Ti alloy*, Metallurgical and Material Transactions, **27A**, 3066–3073, 1996.

http://rcin.org.pl

48. Y. GEFEN, A. HALWANY and M. ROSEN, *Effect of hydrostatic pressure on the cubic-orthorhombic phase transformation in Au-47.5 at % Cd alloy*, Philosophical Magazine, **28**, 1–9, 1973.

49. N. NAKANISHI, T. MORI, S. MIURA, Y. MURAKAMI and S. KACHI, *Pseudoelasticity in Au-Cd thermoelastic martensite*, Philosophical Magazine, **28**, 277–292, 1973.

50. T. KAKESHITA, Y. YOSHIMURA, K. SHIMUZU, S. ENDO, Y. AKAHAMA and F.E. FUJITA, *Effect of hydrostatic pressure on martensitic transformations in Cu-Al-Ni shape memory alloys*, Transactions of Japan Institute of Metals, **29**, 10, 781–789, 1988.

51. K. TSUCHIYA and K. MARUKAWA, *The mechanism of Rubber-like behavior in Cu-Zn-Al martensite*, J. de Physique IV, C8, **5**, 901–905, 1995.

Received January 13, 1999.

http://rcin.org.pl